Optics & Laser Technology 182 (2025) 112097

Contents lists available at ScienceDirect

Optics and Laser Technology

journal homepage: www.elsevier.com/locate/optlastec

Full length article

An alexandrite laser system for positronium laser cooling

N. Gusakova [a,b], A. Camper [c,*], R. Caravita [d], L. Penasa [d,e], L.T. Glöggler [a], T. Wolz [a], V. Krumins [a,f], F.P. Gustafsson [a], S. Huck [a,g], M. Volponi [a,d,e], B. Rienäcker [h], G. Khatri [i], J. Malamant [c], S. Mariazzi [d,e], R.S. Brusa [d,e], L. Cabaret [j], D. Comparat [k], M. Doser [a]

[a] Physics Department, CERN, 1211 Geneva 23, Switzerland
[b] Department of Physics, NTNU, Norwegian University of Science and Technology, Trondheim, Norway
[c] Department of Physics, University of Oslo, Sem Sælandsvei 24, 0371 Oslo, Norway
[d] TIFPA/INFN Trento, via Sommarive 14, 38123 Povo, Trento, Italy
[e] Department of Physics, University of Trento, via Sommarive 14, 38123 Povo, Trento, Italy
[f] University of Latvia, Department of Physics, Raina boulevard 19, LV-1586 Riga, Latvia
[g] Institute for Experimental Physics, Universität Hamburg, 22607 Hamburg, Germany
[h] Department of Physics, University of Liverpool, Liverpool L69 3BX, UK
[i] Systems Department, CERN, 1211 Geneva 23, Switzerland
[j] Berilia Laser SAS, 14 La Légeardière, 49120 Chemillé en Anjou, France
[k] Université Paris-Saclay, CNRS, Laboratoire Aimé Cotton, 91405, Orsay, France

ARTICLE INFO

Keywords:
Laser cooling
Positronium
Alexandrite
Volume Bragg grating

ABSTRACT

We report on a Q-switched alexandrite based ~100 ns long pulse duration ultra-violet laser system. The central wavelength of the fundamental pulse is set by a Volume Bragg Grating in reflection and can be tuned between 728 nm and 742 nm. The spectral bandwidth is ~130 GHz. This laser system was designed in view of Doppler cooling of a cloud of a near room temperature positronium by strongly saturating the 1^3S–2^3P transition. In addition, we report on the development of a KD*P Pockels cell driver designed to both Q-switch the cavity and induce a sharp falling edge of the laser pulse so that the end of the positronium-laser interaction time can be controlled with nanosecond precision.

Positronium (Ps) is the bound state of an electron and its antiparticle, a positron. Being a purely leptonic two-body system with an electronic structure similar to that of hydrogen with just a factor two smaller reduced mass, Ps is an ideal testing ground for quantum electrodynamics through precision spectroscopy [1]. One of the key aspects to reach higher accuracy in the experimental measurement of the Ps transition frequencies is the availability of cold Ps sources [2]. Ps Doppler cooling along the 1^3S–2^3P transition [3–6] stems out as one of the most promising techniques to reach kelvin level temperatures.

Three conditions make laser cooling of positronium a challenging experiment from the laser design point of view. First, the 1^3S–2^3P transition wavelength is in the deep UV range at 243 nm, where laser pulses are much more challenging to generate than the optical wavelength range typical of most laser cooling transitions of alkali atoms. Second, the annihilation lifetime of ground-state ortho-Ps (parallel spin orientation) is just 142 ns, which sets the timescale over which laser cooling has to happen. Third, the temperature at which Ps is produced by typical positron-positronium converters [7] is in the 300 K range, leading to Doppler-broadened transition lines of about 500 GHz [8]. Due to the scarcity of positronium [9], it is not advisable to employ destructive cooling techniques (such as laser-assisted evaporative cooling [10]). Consequently, the laser cooling scheme should be designed so that the largest possible fraction of the initial Doppler profile is covered. Finally, one last technical challenge arises from the use of long laser pulses with slow falling edges: the end of the positronium-laser interaction is poorly defined and part of the atoms might still be in the 2^3P excited state when probing the Doppler profile of the laser-cooled sample. To gain control over the end of the laser–Ps interaction and ensure that all atoms are back in the ground state when measuring the Doppler profile of the laser-cooled sample, it is necessary to have nanosecond time scale precision over the falling edge of the pulse. According to recent simulations based on full diagonalization of the Stark and Zeeman Hamiltonian and a kinetic Monte Carlo algorithm solving exactly the rate equations [6], the laser parameters meeting the above requirements are: order of 10 kW power, 100 ns pulse duration, ~100 GHz spectral bandwidth range. With hundreds of ns long Q-switched pulses and tens to hundreds of mJ of energy per pulse in the 700 nm to 820 nm

* Corresponding author.
E-mail address: antoine.camper@fys.uio.no (A. Camper).

https://doi.org/10.1016/j.optlastec.2024.112097
Received 12 April 2024; Received in revised form 22 October 2024; Accepted 7 November 2024
Available online 27 November 2024

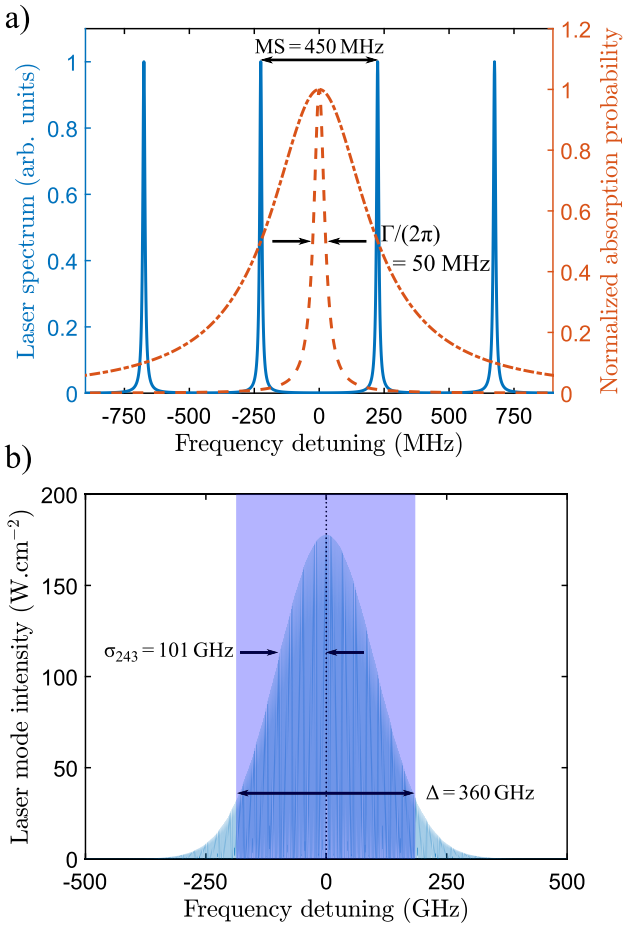

Fig. 1. Illustration of power broadening. (a) The dashed line represents the natural line width of the $1^3S \rightarrow 2^3P$ transition in the absence of power broadening. The dot-dashed line represents the absorption line in the presence of a laser field with intensity $36\,W\,cm^{-2}$ for which the line width matches the MS = 450 MHz mode spacing of the laser. The solid line is a zoomed-in sketch of the laser spectral mode structure. (b) Representation of the intensity distribution in the different laser modes. The area under the spectral envelope appears to be filled by the narrow laser modes spaced by 450 MHz. The bandwidth across which the intensity in a single mode is sufficient (larger than $36\,W\,cm^{-2}$) to broaden the transition line width to at least the laser mode spacing is marked by the light blue area and is 360 GHz large.

range, alexandrite [11,12] is a well-suited laser gain medium for this purpose. In particular, alexandrite has a lower stimulated emission cross-section and therefore emits longer laser pulses than Cr:LiSAF and Ti:sapphire, also considered as candidate active media for Ps cooling laser systems [13–16].

In the present study, we report on the alexandrite-based laser system we developed to meet these requirements and give an in-depth description of the high-voltage switch designed to control the chopping of the laser's falling tail with nanosecond precision. Thanks to a volume Bragg grating spectral filter, a large spectral bandwidth effectively covering the broad initial velocity distribution of Ps is achieved. This laser system was a key element of the recent experimental demonstration of Ps laser cooling [17].

1. Ps cooling in the deep saturation regime

In order to overcome the outlined challenges, we designed a laser system generating pulses with a duration of the order of the ortho-positronium annihilation lifetime (142 ns) and enough energy to saturate the 1^3S–2^3P transition across a $\simeq 10\,mm^2$ area which is determined by the typical dimensions of the Ps cloud [18]. The saturation intensity of this transition is given by Zimmer et al. [6]:

$$I_{sat.} = \frac{1}{6}\hbar c \left(\frac{2\pi}{\lambda}\right)^3 \frac{\Gamma}{2\pi} \tag{1}$$

where $\Gamma = \frac{1}{3.2ns}$ and $\lambda = 243$ nm, yielding $I_{sat.} = 0.45\,W\,cm^{-2}$. Reaching the saturation intensity is however not enough to efficiently laser cool positronium as the spectrum of a multi-longitudinal mode pulsed laser presents large gaps between individual laser gain modes (typically $3\times\frac{c}{2L} = 450$ MHz at 243 nm for a L = 1 m optical length of the oscillator lasing at 729 nm, as shown in Fig. 1a). The linewidth of the 1^3S–2^3P transition being 50 MHz [19], only $\sim$ 10% of the atoms potentially covered by the laser spectrum would actually take part in the cooling process. A solution to this problem is to generate laser pulses with enough energy so that power broadening of the line fills in the gaps between individual laser gain modes [19]. To enlighten this approach, the spectral envelope is described by a Gaussian function so that the power in the nth individual laser mode can be estimated as:

$$P_n = P\,\frac{MS}{\sigma_{243}\sqrt{2\pi}}\exp\left(-\frac{(n\cdot MS)^2}{2\sigma_{243}^2}\right) \tag{2}$$

where P is the total available power, σ_{243} =101(3) GHz is the experimentally achieved width of the envelop of the 243 nm spectrum (see Fig. 2), n is indexing the single laser gain modes (n = 0 is the mode closest to the center of the envelop) and MS (mode spacing determined by the cavity free spectral range; here MS = 450 MHz at 243 nm) corresponds to the frequency interval separating the maxima of two individual laser gain modes. The power broadened line width Γ_n is given by:

$$\Gamma_n = \Gamma\sqrt{1+\frac{P_n}{P_{sat}}}\,, \tag{3}$$

where $\Gamma = \frac{1}{3.2ns} = 2\pi(50\,MHz)$ is the spectral line width of the transition in the absence of power broadening and P_{sat} is the saturation power. In Fig. 1 (a), the red dot-dashed line represents the transition line broadened in the presence of a laser field with intensity $36\,W\,cm^{-2}$ for which the line width matches exactly the laser spectral mode spacing for the laser parameters considered in this study. Given the value of I_{sat} derived above and a total power corresponding to an intensity of the order of $100\,kW\,cm^{-2}$ (the energy of one laser pulse is 1 mJ and the laser beam covers an area of $10\,mm^2$), the highest index for which the power broadened line width Γ_n equals the free spectral range is $n_{max} = 400$. As illustrated in Fig. 1(b), the transition can be saturated for all atoms in an equivalent range $\Delta = 360$ GHz. According to [6], this should allow for cooling a large fraction of a velocity distribution with typical width $5\times10^4\,m\,s^{-1}$ [20] corresponding to a Doppler broadening of 200 GHz.

2. The alexandrite oscillator

A general scheme of the laser system is presented in Fig. 3. An anti-reflection coated C-cut alexandrite laser rod Cr(0.15 at.%):$BeAl_2O_4$ featuring plane-plane end faces is used as the gain medium. The dimensions of the laser rod with horizontally oriented b-axis are 114 mm in length and 6 mm in diameter. The laser crystal is pumped with two 450 Torrs xenon flashlamps with a maximum discharge energy of 160 J. The plane parallel laser resonator consists of a flat high-reflectivity (HR) mirror and an output coupler with a transmission of 30 % at 729 nm. The laser threshold at 729 nm is reached for a pumping voltage of 1625 V and the slope efficiency at this wavelength is 0.3 % (electrical to optical).

To stabilize the cavity and control the size of the TEM_{00} mode in the presence of thermal lensing, a focusing lens with a focal length of 2 m is placed inside the cavity. The Q-switching operation is achieved by placing a KD*P Pockels cell and a polarizer within the cavity. The total length of the resonator is 90 cm. In the cavity, two pinholes are introduced for fundamental transverse mode selection and preventing off-axis lasing due to inhomogeneities in the gain profile of the rod.

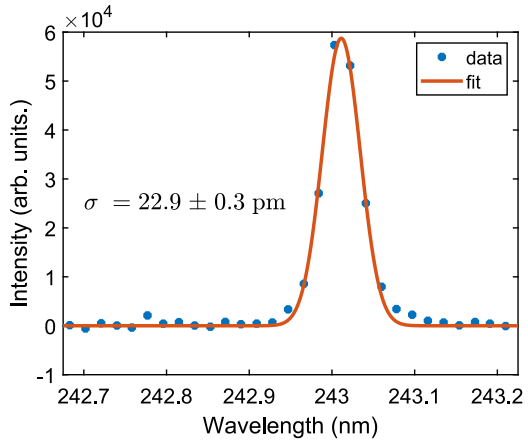

Fig. 2. Single shot spectrum at 243 nm. The width of the spectral envelop σ_{243} = 101(3) GHz is determined by a Gaussian to which the square-root of the variance of the detector pixel size is removed quadratically.

Table 1
Laser parameters.

Energy at 729 nm	up to 40 mJ
Energy at 243 nm	up to 2 mJ (5 % efficiency)
Spectral bandwidth at 730 nm (σ)	130(15) GHz
Spectral bandwidth at 243 nm (σ)	101(3) GHz
Pulse duration at 730 nm (FWHM)	266 ns
Pulse duration at 243 nm (FWHM)	203 ns

To maintain sufficient gain at 729 nm, the laser rod temperature is stabilized at 70 °C with water. We choose a volume Bragg grating (VBG) mounted in a copper holder with passive cooling as the laser wavelength selector due to its high angular selectivity in the desired Ps cooling spectral range (around 729 nm), high diffraction efficiency (>98%) and a relatively high damage threshold (>5 J cm^{-2}, 10 ns). The latter is particularly important considering the energy storage capabilities of alexandrite and the required high output energy of the laser. The bandpass of the VBG (0.4 ± 0.075 nm) is designed to achieve a bandwidth of around 100 GHz after the nonlinear conversion of alexandrite radiation to 243 nm. The values reported in Table 1 correspond to stable working conditions optimized for Ps laser cooling in which a single laser pulse is shot every 110 s. In particular, these parameters allow to saturate the positronium 1^3S–2^3P transition over large spatial areas and cover the atomic cloud for a long period of time.

3. Wavelength tuning

A widespread technique for setting the central wavelength of a tunable laser oscillator is to use multi-plate birefrigent filters [11,13,21,22]. Recently, VBG mirrors [23,24] were introduced as intra-cavity wavelength selectors for continuous wave [25] and pulsed lasers [26], with band pass between 0.1 and 1 nm and high angular selectivity [24]. Here, we use a VBG placed close to the end cavity mirror to set the central wavelength of the laser emission. In order to keep the cavity alignment while tuning the central wavelength, a plane cavity mirror rotating together with the VBG is inserted before the end cavity mirror. The wavelength λ_0 diffracted by the grating varies with the incident angle θ_m (see Fig. 4) following the law:

$$\lambda_0 = 2\Lambda \cdot n_G \cdot \cos(\theta_m) \quad = 2\Lambda \cdot n_G \cdot \cos\left(\varphi + \arcsin\left(\frac{n_{air}\sin(\theta_i)}{n_G}\right)\right) \tag{4}$$

where Λ is the grating period (≈256 nm), n_{air} is the air refractive index and n_G is the glass refractive index (1.487). The details of the VBG design procedure can be found in Ref. Ciapurin et al. [24]. The VBG is used as an intracavity spectral filter. In first approximation, the spectral bandwidth of the light emitted at 729 nm is determined by the spectral acceptance of the VBG (0.4 nm corresponding to 225 GHz FWHM). At 243 nm, the spectral bandwidth is actually limited by the BBO bandwidth acceptance and the crystal length. The small grating tilt φ shown in Fig. 4 is necessary to avoid interference between the beams reflected by the front and back facets and by the grating when used in normal incidence. The parameters of the VBG mirror used in our setup are summarized in Table 2. In practice, the spectral range accessible with this setup covers a range from 728 nm to 742 nm and the wavelength can be set with an absolute accuracy of 10 pm. We measured a linear behavior of the central wavelength emitted by the cavity as a function of the incidence angle θ_i (see Fig. 4) between 728 and 730 nm. A shift of 0.01° in θ_i yields a 23.5 pm (13 GHz) change in the central wavelength. According to Eq. (5), this value is compatible with the central wavelength λ_0 = 729 nm if φ = 0.6° or if Λ = 250 nm.

$$\frac{d\lambda_0}{d\theta_i} = -2\Lambda \cdot n_{air}\frac{\sin(\theta_m)\cdot\cos(\theta_i)}{\cos(\theta_m - \varphi)} \tag{5}$$

In addition, we measure that the standard deviation from the linear behavior is 10 pm. Given the resolution of 4.5″ (22 µrad) for 1/8 step of the stepping motor provided by the manufacturer, the precision on setting the wavelength should rather be of the order of 3 pm. Beyond the fact that the behavior of λ_0 with θ_i is not purely linear, this indicates that other parameters such as fluctuations of the temperature and level of humidity of the ambient air play a role in the accuracy with which the central wavelength of the laser emission can be set.

4. Frequency tripling scheme

The conversion from 729 to 243 nm is achieved by non–linear effects consisting of a doubling stage and the sum frequency of the fundamental and second harmonic referred to as the tripling stage. The doubling stage consists of two 7.5 mm long type I LBO crystals (θ = 90°; ϕ = 39.4°) and the tripling stage of two 7 mm long type I BBO crystals (θ = 50.7°; ϕ = 90°). The temperature of the crystals is actively stabilized to 40 °C. An overall efficiency of about 5 % is achieved at 243 nm which is in reasonable agreement with the expected efficiency given the crystals' length and non-linear susceptibilities. The crystals are used in the walk-off compensating configuration which allows to increase the bandwidth acceptance [27]. The spectral width at 243 nm (see Table 1) estimated by a Gaussian fit is compatible with the mixed acceptance bandwidth of each crystals given by the Select Non-Linear optics (SNLO) software [28] (636 GHz × cm at 365 nm and 104 GHz × cm at 243 nm). The critical phase-matching angle of the crystals is controlled by use of Thorlabs ZFS06 stepper and Z806 brushed motors. In Appendix A, we detail the critical phase-matching equations for uniaxal and biaxial crystals. Making use of Eqs. (A.1) and (A.3), we find that a shift of 45 pm at 365 nm in the phase–matched wavelength is induced by a 0.2 mrad change in the phase–matching angle of the LBO crystals while a shift of 1.9 pm at 243 nm is induced by a 0.2 mrad change in the phase–matching angle of the BBO crystals. The motors used to control the phase-matching angles typically feature a bidirectional repeatability better than 5 µm corresponding to an angle of 135 µrad. With this setup, the uncertainty in selecting the phase-matched central frequency is better than 68 GHz at 365 nm and better than 6.5 GHz at 243 nm. The accuracy allowed by the minimal step size of the motors is potentially up to four orders of magnitude better. The stability of the system is characterized by a standard deviation of 2 GHz on the spectral line width (σ), 1.1 pm (5 GHz) on the central wavelength at 243.056 nm and 13 % on the pulse energy shot-to-shot. The stability of the system was determined by analyzing the properties of a Gaussian fit of each single shot spectrum at 243 nm over the course of 16 h of uninterrupted laser operation.

Based on this reasoning, the selection of a given detuning at 243 nm is automatized. The synchronization of the laser with the rest of the experimental apparatus is achieved with nanosecond time precision by utilizing the ARTIQ/Sinara framework [29] and a LabVIEW-based distributed control system developed at AEgIS [30,31].

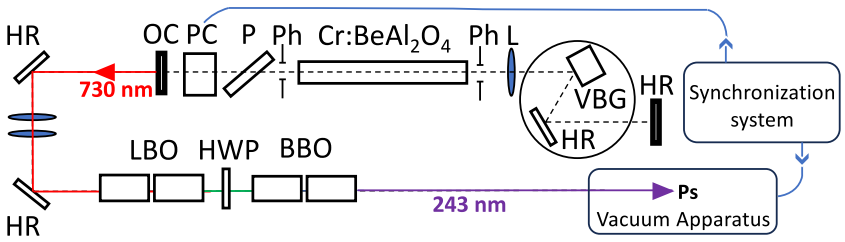

Fig. 3. Scheme of the alexandrite laser system for Ps cooling. The total length of the cavity is 90 cm associated to a 1 m optical length. VBG: Volume Bragg Grating. HR: high reflectivity mirror. Ph: pinhole. L: focusing lens. P: polarizer. PC: Pockels cell. OC: output coupler. BS: Beam splitter. HWP: Half-wave plate. The black circle around the VBG and HR elements represents the platform hosting the two optical elements and mounted on a Standa 8MR151-30 rotation stage (RS). LBO: lithium triborate crystals for second harmonic generation. BBO: β-barium borate crystals for sum frequency generation at the third harmonic frequency.

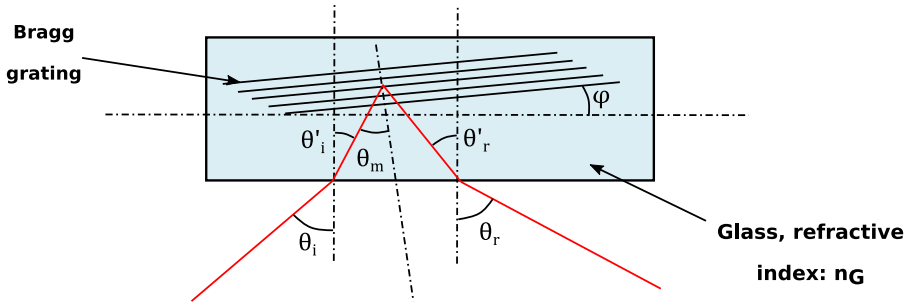

Fig. 4. Volume Bragg grating (VBG) geometry. See Table 2 for values.

Table 2
VBG characteristics.

Manufacturer	Optigrate
Design wavelength (DW)	730 nm in Air at 22 °C
Input Angle at DW (θ_i)	23.3 ± 1 deg
Output Angle at DW (θ_r)	−26.4 ± 1 deg
Diffraction efficiency	>98%
Grating period (Λ)	≃256 nm
Glass refractive index (n_G)	1.487
Grating thickness	1.5 ± 0.3 mm
Spectral Bandwidth (FWHM)	0.4 ± 0.075 nm
Grating tilt (φ)	1 deg

5. HV switch for intracavity pulse chopping

The long laser pulse produced by this cavity has the benefit of a long interaction time with positronium but has the inconvenience of featuring a slow falling tail. Ideally, the laser pulse should have a rectangular shape [15,32] with a falling edge short compared to the spontaneous emission lifetime of the 2^3P excited state (3.2 ns) so that the end of the laser interaction is precisely defined and one can make sure that the atoms have relaxed to the ground state when probing the velocity distribution with the Doppler sensitive $1^3S \rightarrow 3^3P$ two-photon resonant ionization technique making use of few nanosecond long tunable 205 nm and 1064 nm pulses as described in Aghion et al. [33]. For this reason, we developed a Pockels cell driver that allows to both Q-switch the cavity and induce a sharp falling edge of the laser pulse by rapidly closing the cavity during laser emission. A Pockels cell is made of a crystal in which the two refractive indices are affected by the high voltage and, consequently, the beam's polarization state is abruptly changed. When coupled with a polarizer, it plays the role of a fast optical switch. This allows to precisely control the falling edge timing of the laser pulse relative to its triggering time and enables achieving a more square-like pulse shape.

A detailed description of the cost-effective, robust, and highly flexible Pockels cell driver that is implemented in our alexandrite laser system is given in Appendix B. The optimized HV pulse generated by the Pockels cell driver is shown in Fig. 5. It spans from 1160 V to −455 V and has a FWHM of 1.342 µs (see panel a) in Fig. 5. The single-shot temporal profile of the laser was recorded with a 1 ns rise time Thorlabs DET10A/M fast photo-diode. The light pulse generated by the alexandrite laser cavity (red dashed line) is displayed in Fig. 6 with a FWHM pulse duration of 266 ns. Fig. 6 also depicts the HV pulse (solid blue line) used for chopping the light pulse and the chopped laser pulse (solid red line). After chopping, the FWHM of the 729 nm pulse is reduced from 266 ns to 166 ns. The fall time (90%–10%) is approximately 50 ns long. This is almost three times longer compared to the raise time (90%–10%) of the high voltage pulse (see Fig. 5 c) which we attribute to the optimization of the output power of the laser and the piezo-optical relaxation of the crystal. In the future, we plan investigate if this could be compensated for by applying a higher positive HV on the rising edge. The purple dotted line in Fig. 6 shows the laser pulse generated at 243 nm by tripling the 729 nm fundamental. The FWHM of the 243 nm chopped pulse is 122 ns and its falling time (90%–10%) is approximately 43 ns. This time scale represents more than 10 spontaneous emission lifetime. However, the important point is that the timing of the falling edge can be controlled and synchronized with the probe laser with 1 ns precision so that the latter can interact with atoms that have relaxed to the ground state. The long tail observed after the sharp falling edge is attributed to electrical noise. As can be seen on the solid red line, no such long tail is present in the chopped pulse at 729 nm and therefore no light can be generated at 243 nm after the falling edge.

6. Conclusion

We have reported on the laser system we developed to successfully perform positronium laser cooling [17]. In this system, the central laser frequency and subsequent doubling and tripling stages are fully automatized. The use of a VBG as an intra-cavity spectral filter for a long pulse Q-switched cavity and the development of an electronic driver to induce a sharp falling edge are novelties that were crucial to reach the requirements for positronium laser cooling that can also be of interest for other laser applications. In particular, species such as hydrogen [34–38], anti-hydrogen [39–41] and short-lived exotic systems such as muonium [21,42] feature transitions that can be driven by this

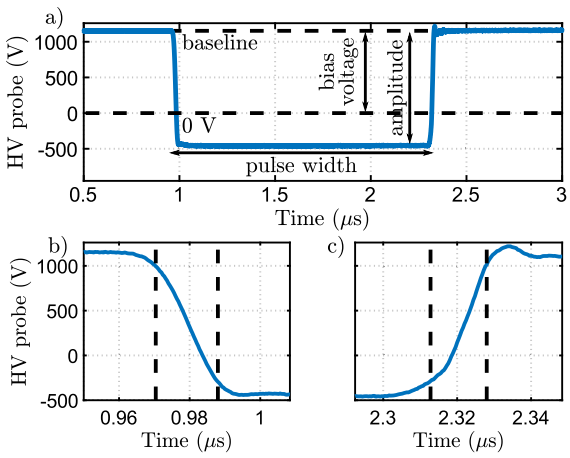

Fig. 5. Measured HV pulse driving the Pockel cells. (a) Shape, (b) fall time (17.7 ns), and (c) rise time (15.2 ns) of the HV pulse driving the LASERMETRICS Q1059PSG-740 Pockels cell, measured using a Lecroy HDO6104 A oscilloscope and an Agilent 10076B probe. The Pockels cell, with a 6pF capacitance, is connected to the pulser output via a high-voltage coaxial cable (Zo = 54 Ω, C = 120 pF/m, length ≈ 40 cm).

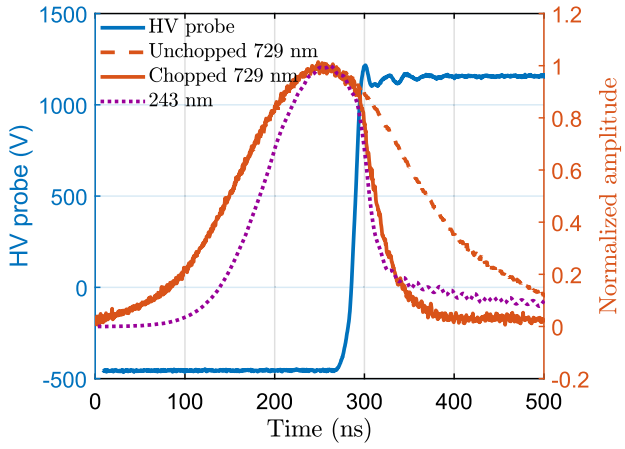

Fig. 6. Chopped and unchopped laser pulses produced by the alexandrite laser. Red dashed line: reference light pulse without chopping at 729 nm. Solid red line: chopped pulse at 729 nm. Purple dotted line: chopped pulse at 243 nm. The fall time (90%–10%) of the 729 nm chopped pulse is 52.3 ns. The solid blue curve shows the high voltage rising edge closing the cavity and causing the sharp falling edge of the laser pulse.

laser system and its harmonics. Spectroscopy and laser manipulation of these compounds could benefit from the developments reported in the present study.

CRediT authorship contribution statement

N. Gusakova: Writing – review & editing, Writing – original draft, Methodology, Investigation, Formal analysis, Data curation, Conceptualization. **A. Camper:** Writing – review & editing, Writing – original draft, Validation, Supervision, Project administration, Methodology, Funding acquisition, Formal analysis, Data curation, Conceptualization. **R. Caravita:** Writing – review & editing, Writing – original draft, Validation, Supervision, Software, Project administration, Methodology, Investigation, Funding acquisition, Formal analysis, Data curation, Conceptualization. **L. Penasa:** Writing – review & editing, Writing – original draft, Validation, Methodology, Investigation, Formal analysis, Data curation, Conceptualization. **L.T. Glöggler:** Writing – review & editing, Investigation, Data curation. **T. Wolz:** Writing – review & editing, Investigation, Data curation. **V. Krumins:** Writing – review & editing, Investigation, Data curation. **F.P. Gustafsson:** Writing – review & editing, Investigation, Data curation. **S. Huck:** Writing – review & editing, Software, Investigation, Data curation. **M. Volponi:** Writing – review & editing, Software, Investigation, Data curation. **B. Rienäcker:** Writing – review & editing, Investigation. **G. Khatri:** Writing – review & editing, Investigation. **J. Malamant:** Writing – review & editing, Software, Investigation. **S. Mariazzi:** Writing – review & editing, Conceptualization. **R.S. Brusa:** Writing – review & editing, Supervision, Funding acquisition. **L. Cabaret:** Writing – review & editing, Writing – original draft, Methodology, Investigation, Formal analysis, Data curation, Conceptualization. **D. Comparat:** Writing – review & editing, Funding acquisition, Conceptualization. **M. Doser:** Writing – review & editing, Supervision, Funding acquisition.

Declaration of competing interest

The authors declare that they have no known competing financial interests or personal relationships that could have appeared to influence the work reported in this paper.

Acknowledgments

This work was supported by the ATTRACT program under grant agreement EU8-ATTPRJ (project O–Possum II); Research Council of Norway under Grant Agreement No. 303337 and NorCC; CERN-NTNU doctoral program; Istituto Nazionale di Fisica Nucleare, Italy; the CERN Fellowship programme and the CERN Doctoral student programme; the EPSRC of UK under grant number EP/X014851/1; European Union's Horizon 2020 research and innovation programme under the Marie Skłodowska-Curie grant agreement ANGRAM No. 748826; Wolfgang Gentner Programme of the German Federal Ministry of Education and Research (grant no. 13E18CHA);

Appendix A. Phase matching equations

The critical phase matching condition is given by:

$$k_3 - k_2 - k_1 = \frac{2\pi c}{n_3\lambda_3} - \frac{2\pi c}{n_2\lambda_2} - \frac{2\pi c}{n_1\lambda_1} = 0 \quad \text{(A.1)}$$

where the indices 1, 2 and 3 refer to the waves being summed (1 and 2) and the resulting wave (3). The wavelength λ_i is associated with the wave vector k_i and the index of refraction n_i, respectively. For type I phase–matching processes, the polarization of 1 and 2 is along the crystal ordinary axis and the polarization of 3 is in the orthogonal plane. For uniaxial crystals such as BBO, the extraordinary index $n_e(\theta)$ is given by:

$$\frac{1}{n_e^2(\theta)} = \frac{\cos^2\theta}{n_o^2} + \frac{\sin^2\theta}{n_e^2} \quad \text{(A.2)}$$

where θ is the angle between the wave normal and the optical axis of the crystal, n_o (respectively n_e) is the ordinary (resp. extraordinary) axis index [43]. For biaxial crystals cut at θ =90° such as the LBO crystals we used, the extraordinary index $n_e(\phi)$ is given by:

$$\frac{1}{n_e^2(\phi)} = \frac{\cos^2\phi}{n_e^2(\phi = 0°)} + \frac{\sin^2\phi}{n_e^2(\phi = 90°)} \quad \text{(A.3)}$$

where ϕ is the angle between the wave normal and the principal axis of the crystal.

Appendix B. Description of the custom pockels cell driver

Electrically, a Pockels cell behaves like a capacitive load ranging from several to tens of picofarads and usually requires a supply voltage in the range of hundreds of volts to several kilovolts. Pockels cell drivers and, in general, fast high voltage pulsers, are typically made using solid state components, such as stacked MOSFETs [44,45] or avalanche transistors [46], and must supply high peak current to rapidly switch a high voltage across the crystal in a matter of nanoseconds or a few tens

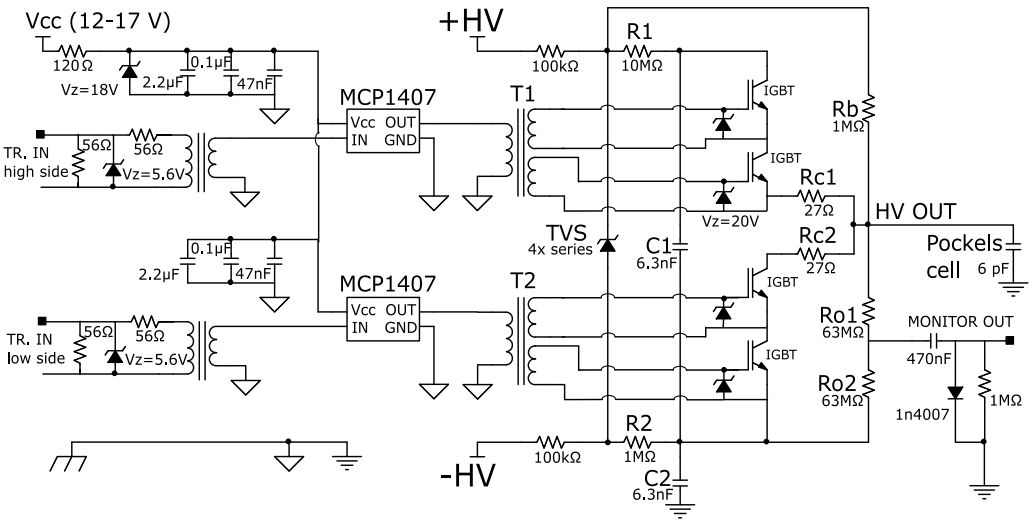

Fig. 7. Schematic of the HV pulser for the Pockel cells.

of nanoseconds. They are typically built in two configurations: an ON-mode, in which a positive or negative voltage is raised to one terminal of the cell, with the other terminal connected to the ground, and an OFF-mode, in which a positive or negative voltage is pulled to ground.

In some cases, as in our laser system, to properly tune the Pockels cell, it is necessary to reverse the voltage polarity applied to one terminal of the crystal from a positive value to a negative one with respect to the other terminal referred to ground. This has proven to be a crucial capability, enabling the compensation of the transient piezo-optical effect within the Pockels cell, which, when the high voltage suddenly decreases, leads to incomplete Q-switch opening and consequent energy losses. In fact, the high voltage applied prior to triggering induces compression in the KD*P crystal, which possesses piezoelectric properties. During the triggering process, the crystal's deformation occurs at a slower rate in comparison to the electro-optical effect, resulting in residual depolarization characterized by stress-induced birefringence [47]. This depolarization can be significantly mitigated by the application of a negative voltage after the triggering event. Consequently, if this negative voltage is not applied, we will have a reduced energy laser pulse and a risk of having high-intensity ringing [48] during and after the pulse. Attempting to address transient depolarization by permanently rotating the crystal would compromise the proper closure of the optical cavity.

The Pockels cell driver (see Fig. 7) works as a fast high-voltage (HV) pulse generator and can drive a capacitive load of up to 50 pF with a negative electric pulse that starts from a positive baseline and has a flat bottom at a negative potential. The amplitude of the electric pulse can be adjusted from 300 V to 2.1 kV and its baseline can be set with a bias voltage ranging from 0 V to 2.1 kV. The pulse width can vary between 600 ns and 15 μs. Both the fall time of the leading edge and the rise time of the trailing edge are approximately 15-18 ns (10%–90%) and are limited solely by the transistor switching speed for a load of 50 pF, as shown in Fig. 5, panels (b) and (c) . The baseline and amplitude of the pulse must be set using two external power supplies connected to the +HV and -HV inputs of the pulser.

In the present setup, two channels of a CAEN Mod.N470 with a current limit of 300 μA are used for this purpose. The rising and falling edges of the high-voltage pulse can be separately triggered using two control signals with amplitudes of 3.3-5 V on 50 Ω and widths of 100-500 ns. The jitter between the edges of the control signals and the edges of the high-voltage pulse is less than 500 ps. The pulser is designed to match the repetition rate of the alexandrite laser and has been tested at 5 Hz. Higher frequencies can be achieved by exchanging the resistors R1 and R2. The Pockels cell driver presented here utilizes a half-bridge topology [49] that operates in a floating configuration. The half-bridge is comprised of two stages, each consisting of two stacked insulated-gate bipolar transistors (IGBT) serving as fast switching elements. The high side of the bridge drives the rising edge of the pulse, while the low side drives the falling edge. IGBTs are a suitable choice for high voltage pulsed electronics applications because they can handle high pulsed currents, have low conduction and switching losses, and can withstand overloads. Additionally, they typically have a lower input capacitance compared to high-voltage MOSFETs with similar specifications.

Here, four IRG4PH50UPbF IGBTs are utilized based on their key characteristics, which include: Collector-to-Emitter Breakdown Voltage VCES = 1200 V, Input Capacitance C_{ies} = 3600 pF, Pulsed Collector Current ICM = 180 A and Rise Time tr=15 ns. Two ceramic capacitors C1 and C2, rated for a maximum voltage greater than 3 kV, serve to push and pull the fast high peak current to the load and to make the pulser floating. The HV resistors, R1 and R2, limit the charging current of the capacitors C1 and C2, and decouple the high voltage supplies from the output pulse. A voltage divider formed by Rb, Ro1 and Ro2, sets the baseline of the HV pulse. The bulk ceramic resistors Rc1 and Rc2, limit the peak current passing through the transistors to about 80 A and protect them in the event of an incorrect operation, where both sides of the half-bridge are simultaneously triggered. Given that the pulser is floating, operates at high voltage, and is made up of stacked elements, it is difficult to drive the IGBTs effectively. The proposed design employs an MCP1407 Microchip gate driver and a custom isolation transformer [50] (T1,T2) to control each side of the half-bridge. The transformer is made using a ferrite toroid with a primary coil connected to the output of the MCP1407 and two twin secondary coils that are tuned to charge the transistor gates as quickly as possible at the same time. A matching network, which serves as galvanic isolation and adapts the impedance to 50 Ω is placed between the trigger signal input and each gate driver. To protect the IGBTs from overvoltage due to incorrect settings of the HV power supplies or high voltage reflected waves from the load, a series of transient voltage suppressors (TVS) have been inserted across the half-bridge from rail to rail. The power supply input of the two MCP1407s has also been protected against overvoltage by a Zener diode. The pulser features a monitor output that allows for the acquisition of a negative pulse with an amplitude up to 8 V on a standard channel of an oscilloscope, which is terminated at 1 MΩ. The monitor signal can be used to verify the amplitude and synchronization of the main HV pulse.

The designed driver, furthermore, bridges the gap between a standard Q-switch driver and a pulse-picker driver [51,52]. The first generates a long electric pulse (up to microseconds) with a fast leading edge

followed by a slow trailing edge. A pulse-picker driver, on the other hand, produces short electrical pulses (tens to hundreds of nanoseconds) at a high repetition rate (MHz) to extract certain laser pulses from a laser burst [53]. Moreover, the proposed design generates bipolar pulses where the baseline, amplitude, and width are arbitrary and adjustable within a wide range of values rather than simply scalable [54] by modifying the circuit. Recently, bipolar high-voltage pulsers in a more demanding configuration have been proposed using SiC MOSFETs [55]. Fig. 5, panel (a) , illustrates the output electric pulse utilized for optimal tuning of the Pockels cell in the current laser system.

Data availability

Data will be made available on request.

References

[1] G. Adkins, D. Cassidy, J. Pérez-Ríos, Precision spectroscopy of positronium: Testing bound-state QED theory and the search for physics beyond the Standard Model, Phys. Rep. 975 (2022) 1–61, http://dx.doi.org/10.1016/j.physrep.2022.05.002.

[2] D.B. Cassidy, Experimental progress in positronium laser physics, Eur. Phys. J. D 72 (2018) 53, http://dx.doi.org/10.1140/epjd/e2018-80721-y.

[3] E.P. Liang, C.D. Dermer, Laser cooling of positronium, Opt. Commun. 65 (6) (1988) 419–424, http://dx.doi.org/10.1016/0030-4018(88)90116-2.

[4] H. Iijima, T. Asonuma, T. Hirose, M. Irako, T. Kumita, M. Kajita, K. Matsuzawa, K. Wada, Laser cooling system of ortho-positronium, Nucl. Instrum. Methods Phys. Res. A 455 (1) (2000) 104–108, http://dx.doi.org/10.1016/S0168-9002(00)00714-2.

[5] K. Shu, X. Fan, T. Yamazaki, T. Namba, S. Asai, K. Yoshioka, M. Kuwata-Gonokami, Study on cooling of positronium for Bose–Einstein condensation, J. Phys. B. 49 (10) (2016) 104001, http://dx.doi.org/10.1088/0953-4075/49/10/104001.

[6] C. Zimmer, P. Yzombard, A. Camper, D. Comparat, Positronium laser cooling in a magnetic field, Phys. Rev. A 104 (2021) 023106, http://dx.doi.org/10.1103/PhysRevA.104.023106.

[7] S. Mariazzi, P. Bettotti, S. Larcheri, L. Toniutti, R.S. Brusa, High positronium yield and emission into the vacuum from oxidized tunable nanochannels in silicon, Phys. Rev. B 81 (2010) 235418, http://dx.doi.org/10.1103/PhysRevB.81.235418.

[8] M. Antonello, A. Belov, G. Bonomi, R.S. Brusa, M. Caccia, et al., AEgIS Collaboration, Rydberg-positronium velocity and self-ionization studies in a 1T magnetic field and cryogenic environment, Phys. Rev. A 102 (2020) 013101, http://dx.doi.org/10.1103/PhysRevA.102.013101.

[9] B. Rienäcker, S. Mariazzi, L. Povolo, F. Guatieri, R. Caravita, L. Penasa, F. Pino, G. Nebbia, R. Brusa, Method for measuring positron number in high intensity nanosecond positron bunches based on Poisson statistic, Nucl. Inst. Meth. A 1033 (2022) 166661, http://dx.doi.org/10.1016/j.nima.2022.166661.

[10] G. Cerchiari, P. Yzombard, A. Kellerbauer, Laser-assisted evaporative cooling of anions, Phys. Rev. Lett. 123 (2019) 103201, http://dx.doi.org/10.1103/PhysRevLett.123.103201.

[11] J. Walling, O. Peterson, H. Jenssen, R. Morris, E. O'Dell, Tunable alexandrite lasers, IEEE J. Quantum Electron. 16 (12) (1980) 1302–1315, http://dx.doi.org/10.1109/JQE.1980.1070430.

[12] D.B. Cassidy, H.W.K. Tom, A.P. Mills, Fundamental physics with cold positronium, AIP Conf. Proc. 1037 (2008) 66, http://dx.doi.org/10.1063/1.2977858.

[13] M. Brown, Increased spectral bandwidths in nonlinear conversion processes by use of multicrystal designs, Opt. Lett. 23 (20) (1998) 1591–1593, http://dx.doi.org/10.1364/OL.23.001591.

[14] K. Yamada, Y. Tajima, T. Murayoshi, X. Fan, A. Ishida, T. Namba, S. Asai, M. Kuwata-Gonokami, E. Chae, K. Shu, K. Yoshioka, Theoretical analysis and experimental demonstration of a chirped pulse-train generator and its potential for efficient cooling of positronium, Phys. Rev. Appl. 16 (2021) 014009, http://dx.doi.org/10.1103/PhysRevApplied.16.014009.

[15] K. Shu, N. Miyamoto, Y. Motohashi, R. Uozumi, Y. Tajima, K. Yoshioka, Development of a laser for chirp cooling of positronium to near the recoil limit using a chirped pulse-train generator, Phys. Rev. A 109 (2024) 043520, http://dx.doi.org/10.1103/PhysRevA.109.043520.

[16] K. Shu, Y. Tajima, R. Uozumi, N. Miyamoto, S. Shiraishi, T. Kobayashi, A. Ishida, et al., Cooling positronium to ultralow velocities with a chirped laser pulse train, Nature (2024) http://dx.doi.org/10.1038/s41586-024-07912-0.

[17] L.T. Glöggler, N. Gusakova, B. Rienäcker, A. Camper, R. Caravita, et al., AEgIS Collaboration Collaboration, Positronium laser cooling via the $1^3S–2^3P$ transition with a broadband laser pulse, Phys. Rev. Lett. 132 (2024) 083402, http://dx.doi.org/10.1103/PhysRevLett.132.083402.

[18] S. Aghion, C. Amsler, A. Ariga, T. Ariga, A. Belov, G. Bonomi, et al., AEgIS collaboration, Positron bunching and electrostatic transport system for the production and emission of dense positronium clouds into vacuum, Nuc. Instrum. Meth. Phys. Res. B 362 (2015) 86–92, http://dx.doi.org/10.1016/j.nimb.2015.08.097.

[19] D.B. Cassidy, T.H. Hisakado, H.W.K. Tom, A.P. Mills, Efficient production of Rydberg positronium, Phys. Rev. Lett. 108 (2012) 043401, http://dx.doi.org/10.1103/PhysRevLett.108.043401.

[20] S. Mariazzi, et al., AEgIS Collaboration, High-yield thermalized positronium at room temperature emitted by morphologically tuned nanochanneled silicon targets, J. Phys. B 54 (2021) 085004, http://dx.doi.org/10.1088/1361-6455/abf6b6.

[21] P. Bakule, P. Baird, M. Boshier, S. Cornish, D. Heller, K. Jungmann, I. Lane, V. Meyer, P. Sandars, W. Toner, M. Towrie, J. Walling, A chirp-compensated, injection-seeded alexandrite laser, Appl. Phys. B 71 (2000) 11–17, http://dx.doi.org/10.1007/PL00021153.

[22] P. Qing, X. Yang, Long pulse, high energy output at 365 nm from an frequency-doubled alexandrite laser, Opt. Commun. 200 (1) (2001) 309–314, http://dx.doi.org/10.1016/S0030-4018(01)01586-3.

[23] C. Voigtländer, D. Richter, J. Thomas, A. Tünnermann, S. Nolte, Inscription of high contrast volume bragg gratings in fused silica with femtosecond laser pulses, Appl. Phys. A 102 (2011) 35–38, http://dx.doi.org/10.1007/s00339-010-6065-6.

[24] I.V. Ciapurin, V. Smirnov, D.R. Drachenberg, G.B. Venus, L.B. Glebov, Modeling of phase volume diffractive gratings, part 2: reflecting sinusoidal uniform gratings, Bragg mirrors, Opt. Eng., Bellingham 51 (5) (2012) 1–11, http://dx.doi.org/10.1117/1.OE.51.5.058001.

[25] G. Tawy, A. Minassian, M.J. Damzen, Volume bragg grating locked alexandrite laser, Optics 3 (1) (2022) 53–59, http://dx.doi.org/10.3390/opt3010007.

[26] M. Hemmer, Y. Joly, L. Glebov, M. Bass, M. Richardson, Volume Bragg Grating assisted broadband tunability and spectral narrowing of Ti:Sapphire oscillators, Opt. Express 17 (10) (2009) 8212–8219, http://dx.doi.org/10.1364/OE.17.008212.

[27] A.V. Smith, D.J. Armstrong, W.J. Alford, Increased acceptance bandwidths in optical frequency conversion by use of multiple walk-off-compensating nonlinear crystals, J. Opt. Soc. Am. B 15 (1) (1998) 122–141, http://dx.doi.org/10.1364/JOSAB.15.000122.

[28] A.V. Smith, Crystal Nonlinear Optics: with SNLO Examples, AS-Photonics Albuquerque, NM, USA, 2018, URL: https://as-photonics.com/wp-content/uploads/2020/08/book-preview.pdf.

[29] D. Nowicka, et al., AEgIS Collaboration, Control system for ion Penning traps at the AEgIS experiment at CERN, J. Phys. Conf. Ser. 2374 (2022) 012038, http://dx.doi.org/10.1088/1742-6596/2374/1/012038.

[30] M. Volponi, S. Huck, R. Caravita, J. Zielinski, G. Kornakov, et al., AEgIS Collaboration, CIRCUS: An autonomous control system for antimatter, atomic and quantum physics experiments, EPJ Quantum Technol. 11 (1) (2024) 10, http://dx.doi.org/10.1140/epjqt/s40507-024-00220-6.

[31] M. Volponi, J. Zieliński, T. Rauschendorfer, S. Huck, et al., AEgIS collaboration, TALOS (Total Automation of LabVIEW Operations for Science): A framework for autonomous control systems for complex experiments, Rev. Sci. Instrum. 95 (8) (2024) 085116, http://dx.doi.org/10.1063/5.0196806.

[32] S. Cialdi, C. Vicario, M. Petrarca, P. Musumeci, Simple scheme for ultraviolet time-pulse shaping, Appl. Opt. 46 (22) (2007) 4959–4962, http://dx.doi.org/10.1364/AO.46.004959.

[33] S. Aghion, C. Amsler, A. Ariga, T. Ariga, G. Bonomi, et al., AEgIS Collaboration, Laser excitation of the $n = 3$ level of positronium for antihydrogen production, Phys. Rev. A 94 (2016) 012507, http://dx.doi.org/10.1103/PhysRevA.94.012507.

[34] L. Cabaret, C. Delsart, C. Blondel, High resolution spectroscopy of the hydrogen Lyman-α line stark structure using a vuv single mode pulsed laser system, Opt. Commun. 61 (2) (1987) 116–119, http://dx.doi.org/10.1016/0030-4018(87)90230-6.

[35] I.D. Setija, H.G.C. Werij, O.J. Luiten, M.W. Reynolds, T.W. Hijmans, J.T.M. Walraven, Optical cooling of atomic hydrogen in a magnetic trap, Phys. Rev. Lett. 70 (1993) 2257–2260, http://dx.doi.org/10.1103/PhysRevLett.70.2257.

[36] K. Eikema, J. Walz, T.W. Hänsch, Continuous wave coherent Lyman-α radiation, Phys. Rev. Lett. 83 (1999) 3828–3831, http://dx.doi.org/10.1103/PhysRevLett.83.3828.

[37] J.M. Michan, G. Polovy, K.W. Madison, M.C. Fujiwara, T. Momose, Narrowband solid state vuv coherent source for laser cooling of antihydrogen, Hyperfine Interact. 235 (2015) http://dx.doi.org/10.1007/s10751-015-1186-0.

[38] N. Saito, Y. Oishi, K. Miyazaki, K. Okamura, J. Nakamura, O.A. Louchev, M. Iwasaki, S. Wada, High-efficiency generation of pulsed Lyman–α radiation by resonant laser wave mixing in low pressure Kr-Ar mixture, Opt. Express 24 (7) (2016) 7566–7574, http://dx.doi.org/10.1364/OE.24.007566.

[39] G. Gabrielse, B. Glowacz, D. Grzonka, C.D. Hamley, E.A. Hessels, N. Jones, G. Khatri, S.A. Lee, C. Meisenhelder, T. Morrison, E. Nottet, C. Rasor, S. Ronald, T. Skinner, C.H. Storry, E. Tardiff, D. Yost, D.M. Zambrano, M. Zielinski, Lyman–α source for laser cooling antihydrogen, Opt. Lett. 43 (12) (2018) 2905–2908, http://dx.doi.org/10.1364/OL.43.002905.

[40] C. Amsler, M. Antonello, A. Belov, G. Bonomi, R.S. Brusa, et al., AEgIS Collaboration, Pulsed production of antihydrogen, Commun. Phys. 4, 19 (2399–3650) (2021) http://dx.doi.org/10.1038/s42005-020-00494-z.

[41] C.J. Baker, W. Bertsche, A. Capra, C. Carruth, C.L. Cesar, et al., ALPHA collaboration, Laser cooling of antihydrogen atoms, Nature 592 (2021) 35–42, http://dx.doi.org/10.1038/s41586-021-03289-6.

[42] V. Meyer, S.N. Bagayev, P.E.G. Baird, P. Bakule, M.G. Boshier, A. Breitrück, S.L. Cornish, S. Dychkov, G.H. Eaton, A. Grossmann, D. Hübl, V.W. Hughes, K. Jungmann, I.C. Lane, Y.-W. Liu, D. Lucas, Y. Matyugin, J. Merkel, G. zu Putlitz, I. Reinhard, P.G.H. Sandars, R. Santra, P.V. Schmidt, C.A. Scott, W.T. Toner, M. Towrie, K. Träger, L. Willmann, V. Yakhontov, Measurement of the $1s - 2s$ energy interval in muonium, Phys. Rev. Lett. 84 (2000) 1136–1139, http://dx.doi.org/10.1103/PhysRevLett.84.1136.

[43] W. Steen, Principles of Optics M. Born and E. Wolf, 7th (expanded) edition, Cambridge University Press, Cambridge, 1999, 952pp. ISBN 0-521-64222-1, Opt. Laser Technol. 32 (5) (2000) 385, http://dx.doi.org/10.1016/S0030-3992(00)00061-X.

[44] T.P. Rutten, N. Wild, P.J. Veitch, Fast rise time, long pulse width, kilohertz repetition rate Q-switch driver, Rev. Sci. Instrum. 78 (7) (2007) 073108, http://dx.doi.org/10.1063/1.2757474.

[45] R.J. Baker, B.P. Johnson, Stacking power MOSFETs for use in high speed instrumentation, Rev. Sci. Instrum. 63 (12) (1992) 5799–5801, http://dx.doi.org/10.1063/1.1143366.

[46] A.R. Tamuri, N. Bidin, Y.M. Daud, Nanoseconds switching for high voltage circuit using avalanche transistors, Appl. Phys. Res. 1 (2) (2009) http://dx.doi.org/10.5539/apr.v1n2p25.

[47] R.P. Hilberg, W.R. Hook, Transient elastooptic effects and Q-switching performance in lithium niobate and KD^*P pockels cells, Appl. Opt. 9 (8) (1970) 1939, http://dx.doi.org/10.1364/AO.9.001939.

[48] G. Sinkevicius, A. Baskys, G. Tamošauskas, Active suppression of piezoelectric ringing in pockels cells for laser cavity application, Symmetry 13 (4) (2021) 677, http://dx.doi.org/10.3390/sym13040677.

[49] R. Schnell, Powering the isolated side of your half-bridge configuration, Analog Device (MS-2663-1) (2014) (Available online) URL: https://www.analog.com/media/en/technical-documentation/tech-articles/Powering-the-Isolated-Side-of-Your-Half-Bridge-Configuration-MS-2663-1.pdf.

[50] Y. Xu, W. Chen, H. Liang, Y.-H. Li, F.-T. Liang, Q. Shen, S.-K. Liao, C.-Z. Peng, Megahertz high voltage pulse generator suitable for capacitive load, AIP Adv. 7 (11) (2017) 115210, http://dx.doi.org/10.1063/1.5006827.

[51] A.I. Bishop, P.F. Barker, Subnanosecond Pockels cell switching using avalanche transistors, Rev. Sci. Instrum. 77 (4) (2006) 044701, http://dx.doi.org/10.1063/1.2194472.

[52] C. Yu, H. Kim, S. Jang, T. Kim, S. Son, C. Kwon, H. Cha, Solid state pulsed power modulator with high repetition rate and short pulse width for high-speed pulsed lasers, IEEE Trans. Ind. Electron. 71 (1) (2024) 388–397, http://dx.doi.org/10.1109/tie.2023.3241247.

[53] Z. Zhao, K. Mernick, M. Costanzo, M. Minty, An ultrafast laser pulse picker technique for high-average-current high-brightness photoinjectors, Nucl. Inst. Meth. A 959 (2020) 163586, http://dx.doi.org/10.1016/j.nima.2020.163586.

[54] X.-W. Feng, X.-W. Long, Z.-Q. Tan, Nanosecond square high voltage pulse generator for electro-optic switch, Rev. Sci. Instrum. 82 (7) (2011) 075102, http://dx.doi.org/10.1063/1.3606447.

[55] Y. Wu, W. Liu, J. Chen, X. Sun, T. Zhang, A novel PWM signal-generation strategy for pockels cell drivers, Photonics 10 (8) (2023) 866, http://dx.doi.org/10.3390/photonics10080866.